11th World Congress on Computational Mechanics (WCCM XI)
5th European Conference on Computational Mechanics (ECCM V)
6th European Conference on Computational Fluid Dynamics (ECFD VI)
E. Oñate, J. Oliver and A. Huerta (Eds)

IMPLEMENTATION AND EXPERIMENTAL VALIDATION OF THE SENDOVA-WALTON THEORY FOR MODE-I FRACTURE

LAUREN A. FERGUSON* AND TIMOTHY D. BREITZMAN†

*Air Force Research Laboratory, Wright-Patterson AFB OH,
University of Dayton Research Institute, 300 College Park Avenue, Dayton OH 45469-0060,
e-mail: lauren.ferguson.1.ctr@us.af.mil

†Air Force Research Laboratory, 2941 Hobson Way, Wright-Patterson AFB OH 45433-7750,
e-mail: timothy.breitzman.1@us.af.mil

Key words: Surface tension, Sendova-Walton fracture theory.

Abstract. The Sendova-Walton fracture theory incorporates atomistic effects into a continuum framework by ascribing a surface tension excess property to the fracture surfaces. We are interested in implementing a numerical model of this theory using the finite element method for mode-I quasistatic brittle fracture, for which the theory predicts finite stresses at the crack tips. This is a challenge since the curvature-dependent surface tension yields a weak formulation with higher-order derivatives. We propose an alternative formulation using a Green's function which we implement using nonlocal calculations on standard finite elements. We present some preliminary results of this implementation, as well as those using a simpler constant surface tension, which reduces but does not eliminate the stress singularity at the tips.

To validate the model, we consider a contact problem, rather than the fracture problem, due to the difficulty of obtaining accurate crack shape measurements in fracture experiments. The equilibrium governing equation is the same as in the fracture problem, but the excess property is now ascribed to the free surface outside the contact region. We conducted corresponding nanoindentation experiments on a cured epoxy resin. By comparing the graphs of applied force versus indentation depth, we observe the correlation between the experimental and simulation results.

1 INTRODUCTION

A reliable understanding of material behavior is critical in system design, especially as the development of new complex materials has skyrocketed in the past few decades. While experimental testing is time-consuming and expensive, computational modeling can be an effective tool for predicting material behavior. We are particularly interested in modeling

the fracture process and garnering information about the strength and fracture toughness of a material.

However, modeling fracture is a challenge due to the different mechanisms that dominate material behavior at different length scales. In the bulk, far from the crack surfaces, the material can be modeled as a continuum and standard linear elastic fracture mechanics (LEFM) does an excellent job of predicting the stress and strain fields of the body in this region. However, in a neighborhood of the fracture surfaces, atomic forces begin to dominate material behavior. These forces are not accounted for in the continuum model and the LEFM prediction is erroneous in this region, particularly in its nonphysical prediction of an infinite strain at the crack tips and an elliptical opening crack shape.

Many recent models have tried to incorporate interatomic effects to improve the LEFM prediction, including the quasicontinuum method [1], variational models [2], and the purely atomistic computational molecular dynamics [3]. While these can be accurate at specific length scales under a narrow set of conditions, they cannot be applied universally and they have multiple parameters which need to be adjusted to individual problems. Much of the difficultly lies in their dependence on the simplistic force laws available for determining atomic interactions.

In contrast, the Sendova-Walton fracture theory [4] incorporates atomistic effects into a continuum framework by ascribing a surface tension excess property to the fracture surfaces. In effect, they treat the neighborhood around the fracture surface as a two-dimensional *dividing surface* which is used to approximate the complex mechanics occurring in this region, as first proposed by Gibbs [5] and further developed in [6, 7]. Sendova and Walton show that their theory can correct the inconsistencies of the LEFM model by choosing the surface tension appropriately. In particular, they show that for mode-I brittle fracture, a constant surface tension reduces the square root stress singularity at the crack tip to a logarithmic one and yields a finite-angled opening crack profile. Even more promising, a curvature-dependent surface tension removes the tip stress singularity entirely and predicts a cusp-like opening shape.

Our goal is to develop a numerical simulation of fracture which can accurately predict displacement, strain, and stress everywhere in a material body by using the Sendova-Walton fracture theory. In this paper, we describe our approach to implementing and validating a numerical model of this theory using the finite element method (FEM) for mode-I brittle fracture. This is straightforward to do for constant surface tension, but is a challenge in the curvature-dependent case, for which the weak formulation involves higher-order derivatives. This difficulty may be circumvented by reformulating the offending boundary condition using a Green's function, which we implement using nonlocal calculations on standard finite elements. In addition to presenting the results of our simulation, we discuss our method for validating the model via a corresponding nanoindentation experiment and give some preliminary empirical data for comparison.

2 MODE-I FRACTURE PROBLEM

We consider mode-I fracture in an infinite, two-dimensional (2D), linear elastic body under far-field tensile loading with an included straight, transverse crack of finite length centered at the origin. According to the Sendova-Walton model, the crack interface is treated as a dividing surface with ascribed surface tension. We employ superposition to move the far-field loading σ to the crack surfaces. We also make use of horizontal and vertical symmetry to reduce the problem domain to the upper-right quarter plane. The resulting finite computational domain $Q = [0, b]^2$, which approximates the upper-right quarter plane, is shown below, where b is the body half-length. Note that we have nondimensionalized by Young's modulus and by the half-length of the included crack, so that the undeformed upper-right crack surface is $\Gamma_C = [0, 1] \times \{0\}$.

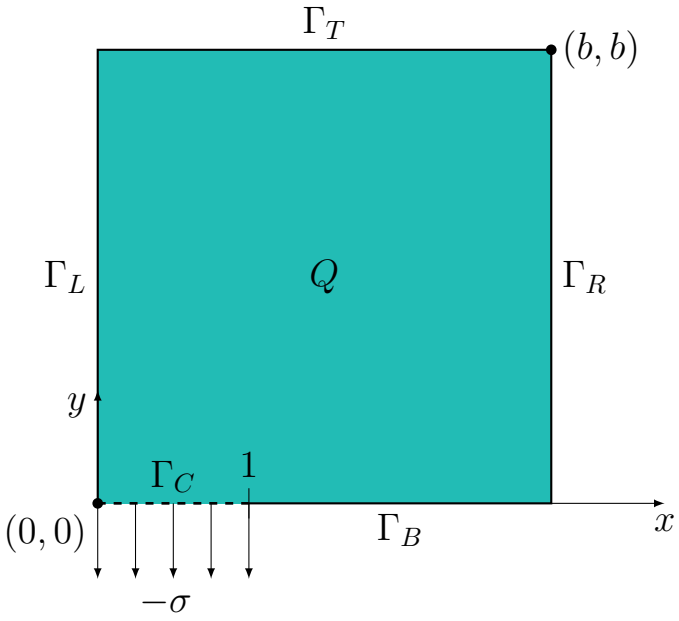

Figure 1: 2D mode-I computational fracture domain Q

To implement this problem using FEM, we first derive the weak formulation using curvature-dependent surface tension (for which constant surface tension is a specialization).

2.1 Governing Equations and Boundary Conditions

Differential momentum balance (DMB) yields the standard equilibrium governing equation for this problem, given by

$$\operatorname{Div} \mathbf{T} = \mathbf{0}, \text{ in } Q, \tag{1}$$

where $\mathbf{T}$ is the stress tensor. For simplicity, we currently neglect body forces. However, we note that it is straightforward to add these in our implementation. We further assume

isotropy, for which the constitutive equation is given by Hooke's law

$$\mathbf{T}(\mathbf{u}) = 2\mu\mathbf{E}(\mathbf{u}) + \lambda\,\mathrm{tr}(\mathbf{E}(\mathbf{u}))\mathbf{I}, \tag{2}$$

where

$$\mathbf{E}(\mathbf{u}) = \frac{1}{2}(\nabla\mathbf{u} + \nabla\mathbf{u}^{\mathsf{T}}) \tag{3}$$

is the linearized strain tensor and $\mathbf{u}$ is the unknown displacement. The material is characterized by its shear modulus μ and elastic constant λ.

We apply symmetry boundary conditions to the left (Γ_L) and bottom (Γ_B) edges, and assume that the top and right edges ($\Gamma_T \cup \Gamma_R$) are traction-free. The linearized curvature-dependent surface tension that is ascribed to the dividing surface is given by

$$\tilde{\gamma}(x) = \gamma_0 + \gamma_1 u_{y,xx}(x,0), \tag{4}$$

where γ_0 and γ_1 are nondimensional constants. As shown in [4, 8], jump momentum balance (JMB) across the upper crack surface (after linearization) requires that

$$\begin{pmatrix}\tau_{xy}\\ \tau_{yy}\end{pmatrix} = \begin{pmatrix}-\gamma_1 u_{y,xxx}\\ -\gamma_0 u_{y,xx}\end{pmatrix}, \quad \text{on } \Gamma_C. \tag{5}$$

Together with the superposed far-field loading, this yields the boundary condition

$$\begin{cases}\tau_{xy} = -\gamma_1 u_{y,xxx}(x,0) & (6)\\ \tau_{yy} = -\gamma_0 u_{y,xx}(x,0) - \sigma & (7)\end{cases}, \quad \text{on } \Gamma_C.$$

2.2 Weak Form

We multiply the DMB (1) by a test function $\mathbf{v}$ and integrate over the domain to obtain the general weak formulation

$$a(\mathbf{u},\mathbf{v}) - \int_{\partial Q} \mathbf{v}\cdot\mathbf{T}\mathbf{n} = 0, \tag{8}$$

where $a(\cdot,\cdot)$ is the standard elastic bilinear term

$$a(\mathbf{u},\mathbf{v}) = \int_Q \mathbf{E}(\mathbf{v}) : \mathbf{C} : \mathbf{E}(\mathbf{u}), \tag{9}$$

and $\mathbf{C}$ is the fourth-order isotropic stress-strain tensor

$$C_{ijkl} = \lambda\delta_{ij}\delta_{kl} + \mu(\delta_{ik}\delta_{jl} + \delta_{il}\delta_{jk}). \tag{10}$$

The boundary term vanishes everywhere except the crack surface, resulting in the weak form given by

$$a(\mathbf{u},\mathbf{v}) + \int_{\Gamma_C} \gamma_0 u_{y,x} v_{y,x} + \int_{\Gamma_C} \tau_{xy}^C\, v_x = \int_{\Gamma_C} \sigma v_y, \tag{11}$$

where we have applied (7) and integration by parts. We use τ_{xy}^C as a placeholder for the JMB condition (6) that must be applied here, but note that it cannot be implemented directly since the resulting integral will have higher order derivatives. Such terms cannot be correctly handled with standard finite elements, which are at most only continuous across element boundaries. Instead, we will reformulate this condition using a Green's function which will eliminate the higher order derivatives. The exception, of course, is when constant surface tension is considered. In this case, both γ_1 and τ_{xy}^C vanish and the weak form is straightforward to implement.

2.3 JMB Reformulation with Green's Function

For the JMB condition (6), we apply Hooke's law, i.e.,

$$-\gamma_1 u_{y,xxx} = \tau_{xy}^C = \mu\big[u_{x,y} + u_{y,x}\big], \tag{12}$$

and rearrange terms to obtain

$$-u_{y,xxx}(x,0) - \frac{\mu}{\gamma_1} u_{y,x}(x,0) = \frac{\mu}{\gamma_1} u_{x,y}(x,0). \tag{13}$$

This can be viewed as a second-order linear ordinary differential equation for $u_{y,x}$ on the interval $\Gamma_C = \{0 \le x \le 1\}$. Symmetry conditions and regularization at the crack tip require that

$$u_{y,x}(0,0) = u_{y,x}(1,0) = 0. \tag{14}$$

Thus the solution to (13) is the solution to the following boundary value problem (BVP).

Definition 1 (Two-point BVP for $u_{y,x}$)**.** *Find $y(x)$ solving*

$$\begin{cases} \mathcal{L}\{y\}(x) = f(x) & (15) \\ y(0) = y(1) = 0 \,, & (16) \end{cases}$$

where $\mathcal{L}\{\cdot\}$ is the second-order, linear differential operator

$$\mathcal{L}\{y\}(x) = -y''(x) - \frac{\mu}{\gamma_1} y(x) \tag{17}$$

and the right-hand-side function is given by

$$f(x) = \frac{\mu}{\gamma_1}\, u_{x,y}(x,0). \tag{18}$$

We let $G(x,q)$ denote the Green's function corresponding to this BVP. Then the solution to (15) is given by

$$u_{y,x}(x,0) = y(x) = \mathcal{G}\{f\}(x) := \int_0^1 G(x,q) f(q) dq. \tag{19}$$

Applying this result and the definition of $f(x)$ to (12) yields the reformulated JMB condition

$$\tau_{xy}^C = \mu \left(u_{x,y} + \frac{\mu}{\gamma_1} \int_0^1 G(x,q)\, u_{x,y}(q,0)\, dq \right), \quad \text{on } \Gamma_C. \tag{20}$$

This condition can viewed as a nonlocal operator acting on the Neumann boundary data $u_{x,y}(x,0)$. In this form, it can be directly applied to the weak form (11) and implemented using standard finite elements (as long as $G(x,q)$ is sufficiently smooth). It remains to compute the Green's function for (15). This will depend on the sign of the constant coefficient in (17). Since the shear modulus μ is always positive, we need only consider the sign of γ_1. (Recall that if γ_1 is zero, we recover the constant surface tension case.) In the following, we set

$$\omega = \sqrt{\frac{\mu}{|\gamma_1|}}. \tag{21}$$

To find the Green's function, we consider the homogeneous equation

$$\mathcal{L}\{y\} = 0, \tag{22}$$

which has a system of solutions satisfying (16) given by

$$y_1(x) = e^{\theta x} - e^{-\theta x}, \tag{23}$$

$$y_2(x) = e^{-\theta(1-x)} - e^{\theta(1-x)}, \tag{24}$$

where we have defined

$$\theta = \begin{cases} \omega i, & \gamma_1 > 0, \\ \omega, & \gamma_1 < 0. \end{cases} \tag{25}$$

This system yields the Wronskian

$$W(y_1, y_2)(q) = 2\theta(e^{\theta} - e^{-\theta}), \tag{26}$$

for which the Green's function is given by

$$G(x,q) = \frac{-1}{2\theta(e^{\theta} - e^{-\theta})} \begin{cases} (e^{\theta q} - e^{-\theta q})(e^{\theta(1-x)} - e^{-\theta(1-x)}), & q \le x \\ (e^{\theta x} - e^{-\theta x})(e^{\theta(1-q)} - e^{-\theta(1-q)}), & x \le q \end{cases}. \tag{27}$$

Together with (20), this completes the definition of the reformulated JMB condition over the crack surface, which no longer has any higher order derivatives. Applying this result to (11) yields the final weak form

$$a(\mathbf{u}, \mathbf{v}) + \int_{\Gamma_C} \gamma_0 u_{y,x} v_{y,x} + \int_{\Gamma_C} \mu v_x u_{x,y} + \int_{\Gamma_C} \frac{\mu^2}{\gamma_1} v_x(x,0) \int_0^1 G(x,q)\, u_{x,y}(q,0)\, dq\, dx = \int_{\Gamma_C} \sigma v_y. \tag{28}$$

2.4 FEM Implementation and Results

We implemented both the constant and curvature-dependent cases described above using FEM and standard bilinear elements. The program was written using the `deal.II` finite element library [9, 10]. In the curvature-dependent case, the weak form (28) involves the double integral term

$$\int_0^1 v_x(x,0) \int_0^1 G(x,q)\, u_{x,y}(q,0)\, dq\, dx \tag{29}$$

whose assembly into the stiffness matrix requires a nonlocal computation (i.e., it must be computed over two distinct elements simultaneously). As the entire assembly is achieved using Gaussian quadrature, this nonlocal term may be computed using the Cartesian product of the 1D quadrature rules, as long as the triangulation is rectangular. One only needs to take care that when transforming to the unit cell via the standard bilinear mapping that the Green's function is still computed on the real cell.

The simulation results for the curvature-dependent case are, unfortunately, not very conclusive. They exhibit numerical instability in the form of oscillations in both the stress field and the crack opening profile. For example, part (a) in Figure 2 below shows the upper-right crack profile for a fixed body half-length of 10, 5% far-field loading, and fixed surface tension parameters $\gamma_0 = \gamma_1 = 1$ as the mesh is adaptively refined (up to 15 refinement cycles). The profiles should be converging as we refine, but this is not the case and in fact the program was unable to find a solution after 11 cycles. In addition to oscillations during the final refinement cycles, we also see that the crack is deforming downward, which would correspond to nonphysical interpenetration of the material across the crack interface.

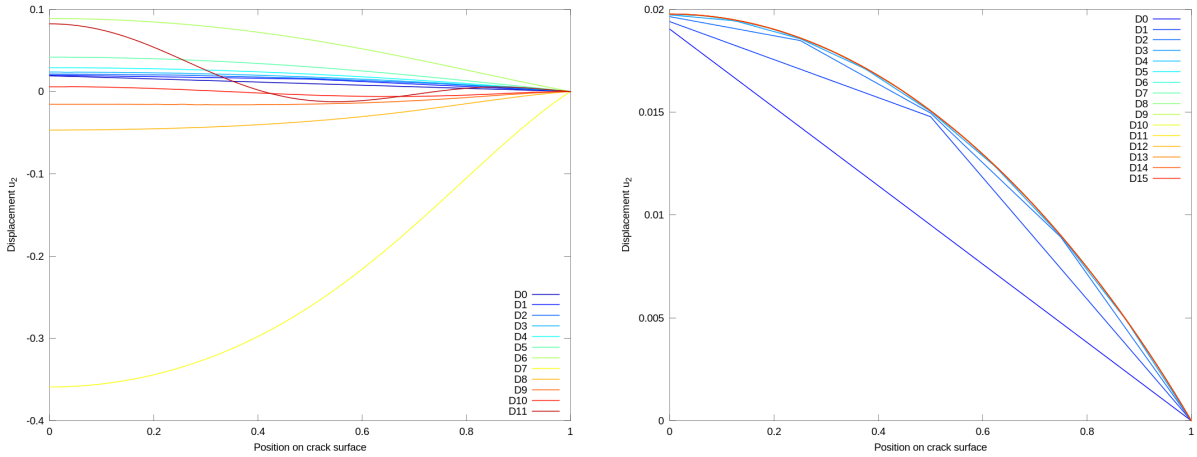

(a) Curvature-dependent

(b) Constant

Figure 2: Crack displacement over refinement for $b = 10$, $\sigma = 0.05$, $\gamma_0 = 1$, (a) $\gamma_1 = 1$, (b) $\gamma_1 = 0$

In contrast, the constant case looks much more promising. Part (b) of the same figure shows the results for the same set of data, except that now $\gamma_1 = 0$. We see very nice convergence as the mesh is refined. We also plot the crack displacement and near-tip stress τ_{yy} for varying γ_0 in Figure 3. Here, the $\gamma_0 = 0$ case recovers the LEFM solution. These results show that as γ_0 increases, we reduce both the stress and the opening angle at the crack tip, as predicted by the theory.

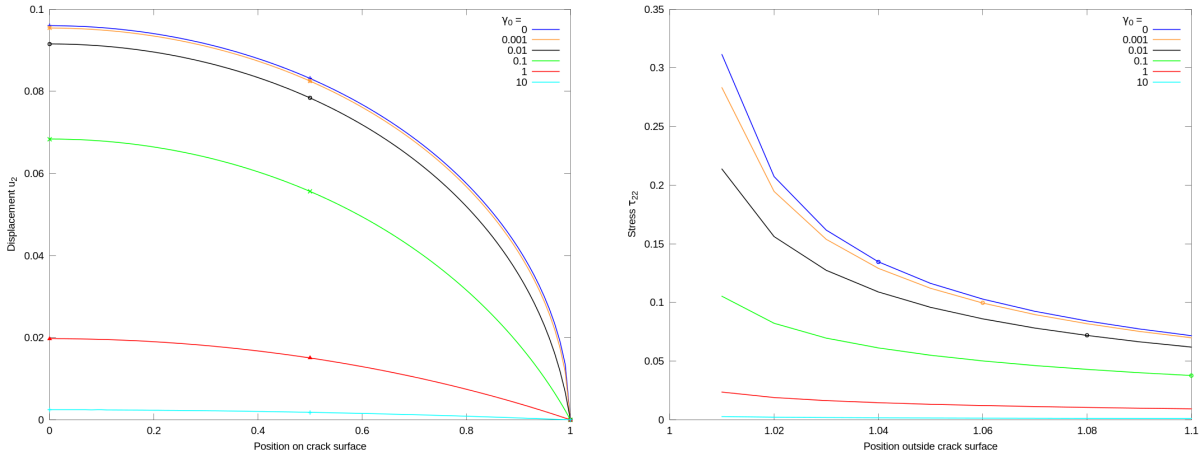

(a) Displacement

(b) Stress

Figure 3: Displacement (a) and near-tip stress τ_{yy} (b) for varying γ_0, with $b = 10$, $\sigma = 0.05$, $\gamma_1 = 0$

3 EXPERIMENTAL VALIDATION

Due to the difficulty of accurately measuring crack profiles in fracture experiments, we have chosen to validate the Sendova-Walton model using a 3D contact problem. We still consider an infinite linear elastic body, but now we fix one face and exert a load on the opposite face using a flat square punch with a specified indentation depth. The equilibrium governing equation is the same as in the fracture problem, but the excess property is now ascribed to the free surface outside the contact region. Figure 4 shows a finite approximation to the 3D domain, where b is the body half-length.

We conducted corresponding nanoindentation experiments on a CYCOM® 5320-1 neat epoxy resin plaque. By comparing the graphs of applied force F versus indentation depth d, we can correlate the experimental and simulation results. Since the F-d curve for the simulation results will depend on surface tension, we can recover the first surface tension parameter for this material by choosing γ_0 such that these curves match with the empirical data. We will present the initial nanoindentation results after a short description of the contact problem.

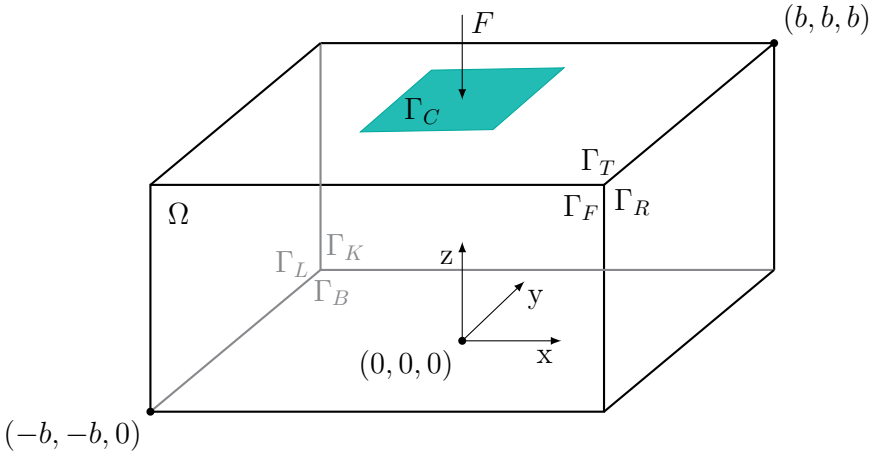

Figure 4: 3D contact finite domain Ω

3.1 Contact Problem Definition

To reduce the number of degrees of freedom required by this problem, we first simplify the contact domain Ω shown in Figure 4 by applying symmetry across the x-z and y-z planes. This reduces the problem to the finite computational domain $Q = [0, b]^3$. We again nondimensionalize by the half-length of the square punch so that the undeformed contact surface is given by $\Gamma_C = [0, 1]^2 \times \{b\}$.

We have the same DMB governing equation (1) and constitutive equation (2) as in the fracture problem. We apply symmetry boundary conditions to the front and left sides of Q and fix the bottom face. We assume the back and right sides are traction-free. For the contact region Γ_C, we specify a fixed indentation depth for the punch and assume that the contact is frictionless. The corresponding total force F exerted by the punch, using symmetry, may be computed by

$$F = 4 \int_{\Gamma_C} \tau_{zz}. \tag{30}$$

Finally, we apply the JMB condition to the top surface outside the contact region. For simplicity, we currently use the constant surface tension model. We conjecture that the logarithmic stress singularity still present in this case will grow so slowly that it will be difficult to observe numerically. The 3D linearized JMB with constant surface tension is given by

$$\begin{cases} \tau_{xz} = 0 \\ \tau_{yz} = 0 \\ \tau_{zz} = \gamma_0(u_{z,xx} + u_{z,yy}) = \gamma_0 \Delta u_z \end{cases}, \text{ on } \Gamma_T \,. \tag{31}$$

We obtain the same general weak formulation (8) as in the fracture problem (neglecting body forces). Applying the boundary conditions above and integrating by parts yields the

weak form

$$a(\mathbf{u}, \mathbf{v}) + \int_{\Gamma_T} \gamma_0 \nabla u_z \cdot \nabla v_z = 0, \tag{32}$$

where $a(\cdot, \cdot)$ is the same bilinear form (9). This formulation is straightforward to implement with FEM, which we have done using `deal.II`.

3.2 Preliminary Experimental and Simulation Results

To validate the results obtained from the simulation described above, we conducted an initial set of nanoindentations on a CYCOM® 5320-1 neat epoxy resin plaque using a Berkovich tip. We used this three-sided pyramid tip, which was already mounted in the nanoindenter, since we expect the F-d curves to be in the same range as a flat tip of the same size. We will do further experiments when a flat tip becomes available. For this initial set, we made 15 indents to a maximum depth of 500 nm (with a minimum effective calculation depth of 180 nm) in a 3x5 grid, with a 50 μm separation between indents. The F-d curves are shown below for each indent for both loading and unloading segments.

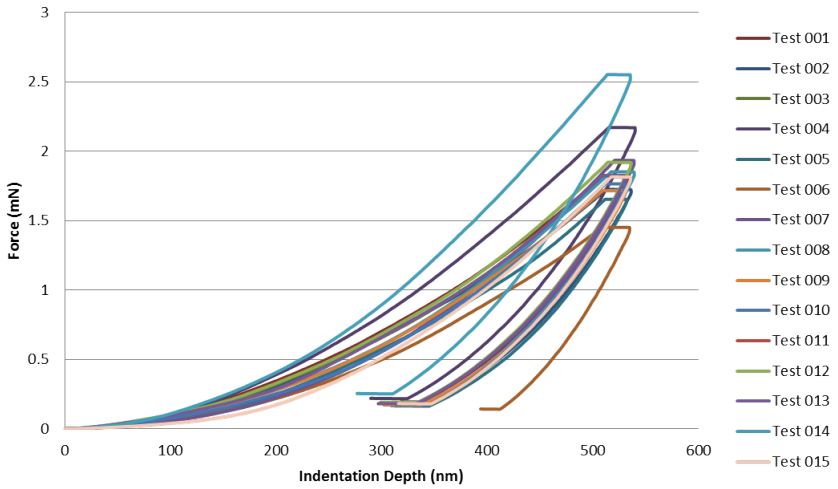

Figure 5: Experimental force vs. depth curves for 15 indents in the epoxy resin plaque

We used the same material properties and nondimensionalized by the indenter size and the Young's modulus to create the corresponding simulation results for this data. However, we quickly ran into memory limitations due to the size of the domain, in which the effective body length is more than 1000 times that of the indenter. On our current platform, we were restricted to body lengths of no more than 20 times the length of the indenter, which also restricted the depth to which we could indent. For this reason, we chose to look at a single indentation depth of 200 μm (corresponding to half the maximum body length) for varying values of the constant surface tension γ_0.

We computed the corresponding force and these results are shown in the table below. For comparison, we also list the nondimensionalized force measured experimentally (averaged over the indents). As you can see, the forces we are able to produce are significantly less than the measured force, with the highest value actually occurring for zero surface tension, which corresponds to the LEFM solution. However, we are more concerned by the fact that simulation shows the material interpenetrating both itself and the sides of the indenter. Since this effect is minimized or eliminated for shallower depths, we conjecture that the interpenetration may be improved by using more accurate domain approximations and finer meshes, or by applying additional constraints to the top and contact surfaces.

Table 1: Computed force for varying γ_0 with $b = 20$, $d = 10$

γ_0	F
0	26.065667017
0.01	23.298329016
0.1	18.877746174
1	13.028430541
10	8.316230257
100	3.809877886
F (measured)	137.9239853

4 CONCLUSION

We have developed a numerical implementation of the Sendova-Walton fracture theory in the case of constant surface tension that is an excellent tool for predicting crack shape and stress and strain fields for mode-I brittle fracture. This implementation also verifies the prediction of the Sendova-Walton model in that it exhibits a finite opening angle and a reduced stress singularity at the crack tip. It has a significant advantage over other models in that it has no adjustable parameters, only requiring information about the material, including the constant surface tension.

In the case of curvature-dependent surface tension, we have implemented a numerical simulation by reformulating the jump momentum balance condition using a Green's function. However, we see that a correct implementation is challenging and ours needs additional development to produce satisfactory results. We are still investigating ways to eliminate the numerical instability exhibited in the results of our simulation. We are also interested in studying when this curvature-dependent case is actually required for precision and under what circumstances the constant case may be sufficient.

For the experimental validation of the Sendova-Walton theory, we have conducted some preliminary nanoindentation experiments corresponding to a contact problem. However, the deeper depths required for experimental comparison require increases in both domain and mesh sizes for accurate results. We plan to run our simulation on a supercomputer

where we can have sufficient memory for these requirements. In addition, we may need to modify the boundary condition at the indenter edge, since treating the material as if it is glued to the indenter may be too rigid, and this may be causing some of the interpenetration seen in the results. We will also conduct more extensive experiments using a flat indenter.

Acknowledgments. This work was supported by the Air Force Office of Scientific Research project 12RX13COR. The authors would like to thank Kevin Tienda for preparing the epoxy resin plaque and Bill Ragland for conducting the nanoindentation experiments. They are also indebted to Dr. Jay Walton and Mallikarjuna Muddamallappa for the idea of using a Green's function reformulation with superposition.

REFERENCES

[1] Miller, R.E. and Tadmor, E.B. Hybrid continuum mechanics and atomistic methods for simulating materials deformation and failure. *MRS Bull.* (2007) **32**(11):920–926.

[2] Bourdin, B., Francfort, G.A., and Marigo, J.-J. The variational approach to fracture. *J. Elasticity* (2008) **91**(1-3):5–148.

[3] Abraham, F.F. The atomic dynamics of fracture. *J. Mech. Phys. Solids* (2001) **49**(9):2095–2111.

[4] Sendova, T. and Walton, J.R. A new approach to the modeling and analysis of fracture through extension of continuum mechanics to the nanoscale. *Math. Mech. Solids* (2010) **15**(3):368–413.

[5] Gibbs, J.W. *The Collected Works of J. Willard Gibbs*, volume I – Thermodynamics. Longmans, Green, and Co., New York (1928).

[6] Slattery, J.C., Oh, E.-S.., and Fu, K.B. Extension of continuum mechanics to the nanoscale. *Chem. Eng. Sci.* (2004) **59**(21):4621–4635.

[7] Oh, E.-S., Walton, J.R., and Slattery, J.C. A theory of fracture based upon an extension of continuum mechanics to the nanoscale. *J. Appl. Mech. - T. ASME* (2006) **73**(5):792–798.

[8] Ferguson, L.A. *Brittle fracture modeling with a surface tension excess property.* Ph.D. dissertation, Texas A&M University, College Station, TX (2012).

[9] Bangerth, W., Hartmann, R., and Kanschat, G. deal.II – A general-purpose object-oriented finite element library. *ACM T. Math. Software* (2007) **33**(4):24/1–24/27.

[10] Bangerth, W., Heister, T., Heltai, L., Kanschat, G., Kronbichler, M., Maier, M., Turcksin, B., and Young, T. The `deal.ii` library, verion 8.0. *arXiv preprint* (2013) `http://arxiv.org/abs/1312.2266v3`.